

ALPHA-RESONANCES IN MEDIUM AND HEAVY NUCLEI

II. Review of microscopic models

D.S. Delion*, V.V. Baran[†], and A. Dumitrescu[‡]

Abstract

We review microscopic approaches describing α -like resonances in nuclei with $Z \geq 50$. We give a microscopic explanation of α -like rotational bands in the $^{40}\text{Ca}+\alpha$ system in terms of single particle Gamow resonances. On the other hand, we show that for α -decaying nuclei the decay width can be described only in terms of a preformed α -cluster, existing on the nuclear surface in addition to the standard mean field cluster. Thus, we use a semi-microscopic hybrid model combining the mean field formation with a preformed α -cluster in order to explain the order of magnitude of the experimental decay width. Finally, we analyze proton-neutron versus α -like correlations.

keywords: alpha decay, resonant state, decay width

<https://doi.org/10.56082/annalsarscipphyschem.2020.1.70>

*delion@theory.nipne.ro ¹ Horia Hulubei National Institute for Physics and Nuclear Engineering, Reactorului 30, P.O. Box MG-6, RO-077125, Bucharest-Măgurele, România; ² Academy of Romanian Scientists, 3 Ilfov RO-050044, Bucharest, România; ³ Bioterra University, 81 Gârlei RO-013724, Bucharest, România; Acknowledgment for financial support: Grant of the Romanian Ministry of Research and Innovation, CNCS - UEFISCDI, PN-19060101/2019-2022;

^{†1} Horia Hulubei National Institute for R&D in Physics and Nuclear Engineering, Str. Reactorului no. 30, P.O. Box MG-6, RO-077125, Bucharest-Măgurele, România; ⁴ Department of Physics, University of Bucharest, 405 Atomistilor, POB MG-11, RO-077125, Bucharest-Măgurele, România;

^{‡1} Horia Hulubei National Institute for R&D in Physics and Nuclear Engineering, Str. Reactorului no. 30, P.O. Box MG-6, RO-077125, Bucharest-Măgurele, România;

1 Introduction

α -particles were first evidenced by the discovery of the α -decay mode more than 100 years ago, marking the birth of nuclear science. The α -decay mode occurs for medium/heavy nuclei with $Z \geq 50$. Its explanation was proposed soon after the establishments of quantum mechanics [1, 2] in terms of the quantum penetration of a preformed α -particle through the Coulomb barrier. The microscopic description of the α -particle preformation [3, 4, 5, 6, 7] still remains a theoretical challenge, due to the fact that a quartet structure, built in terms of a collective superposition between two-proton plus two-neutron single particle orbitals generated by a standard nuclear mean field, underestimates the experimental decay width by two orders of magnitude [8].

First of all, we will give an explanation of α -like rotational bands in the $^{40}\text{Ca}+\alpha$ system in terms of the microscopic α -particle formation amplitude by using single particle Gamow resonances provided by the standard nuclear mean field.

On the other hand, the analysis of decay data between ground states shows that the probability of the α -particle formation on the nuclear surface, estimated by dividing the decay width to the penetration probability, is proportional to the fragmentation potential, given by the difference between the Coulomb barrier and Q -value. This quantity does not enter the standard estimation of the preformation amplitude in terms of single particle orbitals generated by some nuclear mean field. A simple two-body quantum calculation of Ref. [9] clearly shows that this proportionality can be explained by considering a preformed cluster in a pocket-like potential centered on the nuclear surface, i.e. similar to the α -like resonant state seen in light nuclei by scattering experiments.

The aim of this paper is to review the microscopic theoretical approaches concerning the resonant character of the α -decay phenomenon.

2 Microscopic α -formation amplitude

In a microscopic description of the α -decay process the internal part of the α -core potential is replaced by a wave function, seen as a formation amplitude given by the following overlap between initial and final configurations [4, 5]

$$\mathcal{F}(\mathbf{R}) \equiv \langle \alpha D | P \rangle = \int d\mathbf{x}_\alpha d\mathbf{x}_D [\psi_\alpha(\mathbf{x}_\alpha) \Psi_D(\mathbf{x}_D)]^* \Psi_P(\mathbf{x}_P) = \frac{f_{int}(\mathbf{R})}{R}, \quad (2.1)$$

where by \mathbf{x} we denoted the internal coordinates of the fragments. Therefore, the final result depends upon the relative radius between emitted fragments \mathbf{R} . The antisymmetrisation α -core effects are neglected here, because we will estimate this quantity beyond the geometrical touching point (i.e. in the barrier region), where the two fragment have a small geometrical overlap and therefore Pauli effects are strongly diminished. The wave function of the α -particle ψ_α is expressed as a Gaussian in

relative and center of mass coordinates, which is actually a product of the lowest harmonic oscillator (ho) states with the parameter [4]

$$\beta_\alpha = \frac{M_\alpha \omega_\alpha}{\hbar} \sim 0.5 fm^{-2} . \quad (2.2)$$

Theoretical nuclear structure is built on the single particle (sp) mean field concept. Thus, the wave functions of the parent and daughter nuclei in Eq. (2.3) are built as various superpositions of antisymmetrised products between sp orbitals (Slater determinants) generated as eigenstates of some nuclear mean field. The mean field is generated by using the standard Hartree-Fock (HF) selfconsistent procedure for many-body systems above magic nuclei, involving only few valence sp orbitals, and therefore the wave functions of even-even parent/daughter nuclei are Slater determinants built on these orbitals. For superfluid systems between magic nuclei one uses the Hartree-Fock-Bogolyubov quasiparticle method. A more pragmatic approach uses a parametrised mean field with a Woods-Saxon shape.

In the absence of the α -core antisymmetrisation the wave function of the parent nucleus can be approximately factorized as a product between a four-body quartet state and the daughter wave function, i.e.

$$\Psi_P = \Psi_\alpha \Psi_D , \quad (2.3)$$

and therefore the formation amplitude becomes

$$\mathcal{F}_\alpha(\mathbf{R}) = \int d\mathbf{x}_\alpha \psi_\alpha^*(\mathbf{x}_\alpha) \Psi_\alpha \equiv \langle \psi_\alpha | \Psi_\alpha \rangle . \quad (2.4)$$

Typical examples of nuclei with an α -like structure are first of all double-magic plus quartet structures like $^{40}Ca + n\alpha$, $^{100}Sn + n\alpha$, $^{208}Pb + n\alpha$. For $n = 1$, the procedure to estimate the overlap integral (2.4) consists in expanding the quartet in terms of products between pp , nn and pn pairs of sp orbitals. Due to the fact that the above mentioned systems are spherical we can use the angular momentum coupling scheme

$$|\Psi_\alpha\rangle = Q_{I_\nu M_\nu}^\dagger |0\rangle , \quad (2.5)$$

in terms of the quartet operator, given by the following superposition

$$\begin{aligned} Q_{I_\nu M_\nu}^\dagger &= \sum_{J_\mu J'_\mu} Z_{I_\nu}^{(1)}(J_\mu J'_\mu) \left[P_{J_\mu}^\dagger(pp) \otimes P_{J'_\mu}^\dagger(nn) \right]_{I_\nu M_\nu} \\ &+ f \sum_{J_\mu J'_\mu} Z_{I_\nu}^{(2)}(J_\mu J'_\mu) \left[P_{J_\mu}^\dagger(pn) \otimes P_{J'_\mu}^\dagger(pn) \right]_{I_\nu M_\nu} , \end{aligned} \quad (2.6)$$

where I_ν is the quartet spin_{eigenvalue} index. The collective pair operators

$$P_{J_\mu M_\mu}^\dagger(\tau\tau') = \sum_{jj'} X_{J_\mu}(\tau j; \tau' j') \overline{C}_{J_\mu M_\mu}^\dagger(\tau j; \tau' j') , \quad (2.7)$$

depend on the normalized basis pairs, built on sp orbitals

$$\overline{C}_{J_\mu M_\mu}^\dagger(\tau j; \tau' j') = \frac{1}{\sqrt{1 + \delta_{\tau j; \tau' j'}}} \left[c_{\tau j}^\dagger \otimes c_{\tau' j'}^\dagger \right]_{J_\mu M_\mu}, \quad (2.8)$$

where J_μ is the pair spin_{eigenvalue} index. The isospin index is $\tau = p, n$ and the sp orbitals $c_{\tau j m}^\dagger$, generated by the nuclear mean field, depend on spherical quantum numbers $j \equiv (\epsilon, j^\pi)$ (eigenvalue, spin and parity). The X-two-body coefficients are given by the equation of motion procedure with some two-body interaction \widehat{V} .

$$[\widehat{H}, P_{J_\mu M_\mu}^\dagger(\tau \tau')] \equiv [\widehat{T} + \widehat{V}, P_{J_\mu M_\mu}^\dagger(\tau \tau')] = E_{J_\mu}(\tau \tau') P_{J_\mu M_\mu}^\dagger(\tau \tau'). \quad (2.9)$$

By supposing that the basis pairs operators satisfy a boson commutation rule

$$\left[\overline{C}_{J_\mu M_\mu}(\tau_1 j_1; \tau'_1 j'_1), \overline{C}_{J_\mu M_\mu}^\dagger(\tau_2 j_2; \tau'_2 j'_2) \right] = \delta_{1,2}, \quad (2.10)$$

one obtains the standard system of the Tamm-Dankoff Approximation (TDA)

$$\frac{1}{2} \sum_{kk'} \langle \tau j; \tau' j' | \widehat{V} | \tau k; \tau' k' \rangle X_{J_\mu}(\tau k; \tau' k') = [E_{J_\mu}(\tau \tau') - \epsilon_{\tau j} - \epsilon_{\tau' j'}] X_{J_\mu}(\tau j; \tau' j'), \quad (2.11)$$

for $(\tau \tau') = (pp)$, (nn) and (pn) systems. The four-body Z-coefficients are also provided by the equation of motion procedure [10]

$$[\widehat{H}, Q_{I_\nu M_\nu}^\dagger] = \mathcal{E}_{I_\nu} Q_{I_\nu M_\nu}^\dagger. \quad (2.12)$$

By using the equations for pairs (2.9), one obtains the following system for Z

$$\begin{pmatrix} H_{11} & H_{12} \\ H_{21} & H_{22} \end{pmatrix} \begin{pmatrix} Z_{I_\nu}^{(1)} \\ Z_{I_\nu}^{(2)} \end{pmatrix} = \mathcal{E}_{I_\nu} \begin{pmatrix} N_{11} & N_{12} \\ N_{21} & N_{22} \end{pmatrix} \begin{pmatrix} Z_{I_\nu}^{(1)} \\ Z_{I_\nu}^{(2)} \end{pmatrix}, \quad (2.13)$$

where the norm and interaction matrices are defined as follows

$$\begin{aligned} N_{km} &= \langle 0 | \left[P^\dagger(k) \otimes P^\dagger(k') \right]_{I_\nu M_\nu}^\dagger \left[P^\dagger(m) \otimes P^\dagger(m') \right]_{I_\nu M_\nu} | 0 \rangle \\ H_{km} &= \frac{1}{2} [E(k) + E(k') + E(m) + E(m')] N_{km}, \end{aligned} \quad (2.14)$$

in terms on spin-isospin pair index: $1 \equiv (J_\mu pp; J'_\mu nn)$, $2 \equiv (J_\mu pn; J'_\mu pn)$. Their detailed form is given in Ref. [10].

The overlap integral (2.4) can be now estimated for each eigenstate I_ν (2.5) provided by the system (2.13) in a standard way. Namely, the product between two proton and two neutron sp orbitals, entering the expansion (2.6), can be rewritten in terms of relative and center of mass (cm) Moshinsky coordinates in the ho

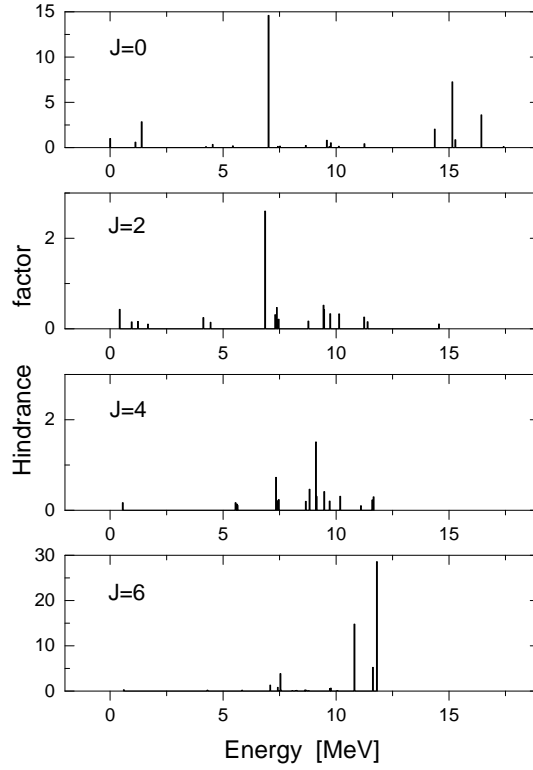


Figure 1: The hindrance factors (2.17) as functions of the excitation energy for $I_\nu^+ = 0_\nu^+, 2_\nu^+, 4_\nu^+, 6_\nu^+$ four-particle eigenstates in the system $^{44}\text{Ti} = ^{40}\text{Ca} + \alpha$ [11].

basis. Finally, the overlap between the α -particle wave function and the resulting ho functions in pp , nn and pn relative coordinates can be written as the following superposition

$$\mathcal{F}_{I_\nu}(\mathbf{R}) \equiv \langle \phi_\alpha | Q_{I_\nu}^\dagger | 0 \rangle = \sum_{N_\alpha L_\alpha} W_{I_\nu}(N_\alpha L_\alpha) \Phi_{N_\alpha L_\alpha}^{(4\beta)}(\mathbf{R}) . \quad (2.15)$$

in terms of radial ho functions depending on cm coordinate of the α -core system and four times the sp ho parameter

$$\beta = \frac{M_N \omega_N}{\hbar} , \quad \hbar \omega_N = 41A^{-1/3} . \quad (2.16)$$

Details are given in Section 5.1, according to Refs. [10, 12]. The nuclear structure information is carried out by the pair of X-coefficients (2.7) and quartet Z-coefficients (2.6). Let us mention here that, according to Eq. (2.15), the α -particle in some state I_ν is born from the ground state by the action of the quartet operator $Q_{I_\nu}^\dagger$. The

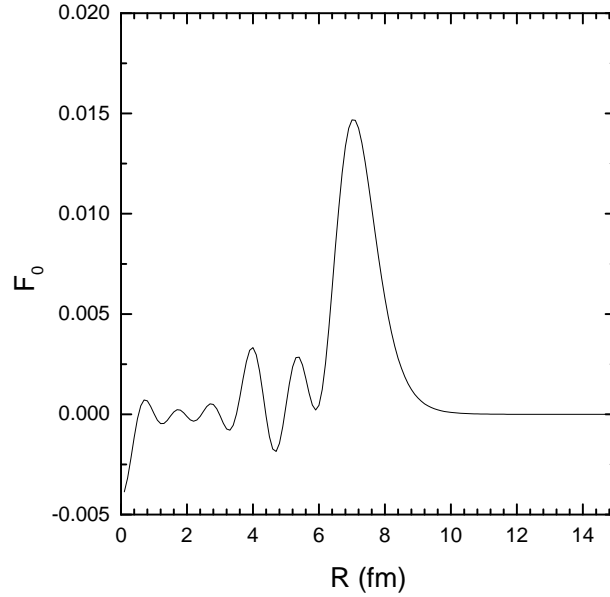


Figure 2: The formation amplitude for the system $^{212}\text{Po} = ^{208}\text{Pb} + \alpha$ versus radius [10].

lowest eigenvalue $I_\nu = 0_1^+$ corresponds to a transition between ground states. The higher excited eigenstates are called **α -like resonant states**.

These states can be probed in light systems by the elastic scattering of α -particles. We estimated their structure for $^{44}\text{Ti} = ^{40}\text{Ca} + \alpha$ in Ref [11]. As sp orbitals were considered all bound and narrow Gamow sp resonances in ^{40}Ca , generated by a Woods-Saxon potential with universal parametrisation. Then pp , nn and pn X-coefficients of the pair excitations were estimated, by using the surface-delta interaction in the TDA system of equations for ^{42}Ti , ^{42}Ca and ^{42}Sc , respectively. The doubly magic nucleus ^{40}Ca was considered as a vacuum state. Finally, the Z-coefficients and the α -formation overlap integral to the quartet eigenstates were computed. They are given in Ref. [11]. In Fig. 1 of the same reference we estimated the “hindrance factors” defined by the ratio

$$HF = \frac{S_{I_\nu^+}}{S_{0_1^+}}, \quad (2.17)$$

between spectroscopic factors

$$S_{I_\nu^+} = \int_0^\infty |\mathcal{F}_{I_\nu^+}(R)|^2 R^2 dR, \quad (2.18)$$

to some excited state I_ν^+ and ground state 0_1^+ . The positions of maximal values

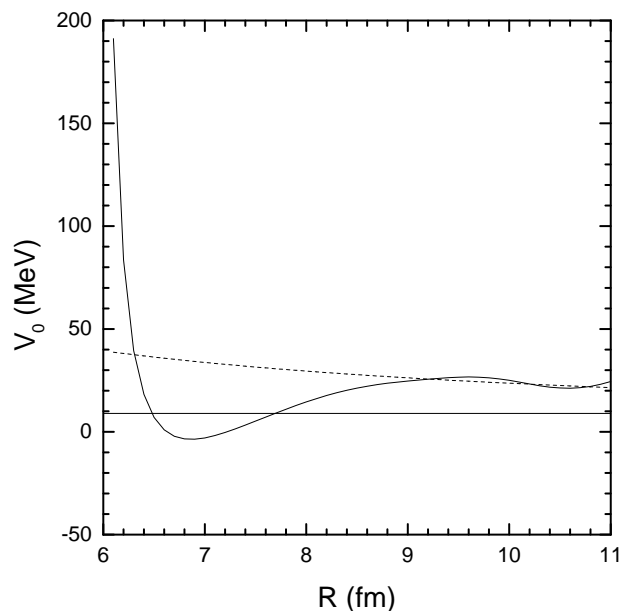


Figure 3: The equivalent local potential of the system $^{212}\text{Po} = ^{208}\text{Pb} + \alpha$ (solid line) and Coulomb interaction (dotted line) [10] versus radius. By a horizontal line is given the Q-value of the α -decay from ^{212}Po [10].

revealed a very good description of the measured quasimolecular resonances, as can be seen in the Table 1.

Table 1. Energies of α -like states in ^{44}Ti [11].

I_{ν}^{+}	E_{exp} (MeV)	E_{th} (MeV)
0_{1}^{+}	0.00	0.00
2_{1}^{+}	6.67	7.01
4_{1}^{+}	7.22	7.13
6_{1}^{+}	7.75	7.34

The microscopic structure of α -resonances was also estimated for $^{212}\text{Po} = ^{208}\text{Pb} + \alpha$ in Ref. [10], where this microscopic method was initially proposed. The low-lying states in ^{210}Po , ^{210}Pb and ^{210}Bi were described as collective superpositions of pairs by using the surface-delta interaction in the TDA system of equations. The double magic nucleus ^{208}Po was considered as a vacuum. We considered sp bound states and narrow Gamow resonances, generated by the Woods-Saxon mean field with universal parameterisation. Theoretical predictions for energies are in a reasonable agreement with experimental data, as can be seen in Table II of Ref. [10]. In spite

of its simplicity, the agreement of energies for low-lying states in ^{212}Po was good, as can be seen in the Table 2.

Table 2. Energies of low-lying states in ^{212}Po [10].

I_ν^+	E_{exp} (MeV)	E_{th} (MeV)
0_1^+	0.000	0.000
2_1^+	0.727	0.949
4_1^+	1.132	1.087
6_1^+	1.355	1.081
8_1^+	1.476	1.131
2_2^+	1.513	1.203
1_1^+	1.621	1.907
2_1^+	1.679	1.783
0_2^+	1.801	2.080
2_4^+	1.806	2.248

Several high-lying α -like states with relative large hindrance factors were predicted to be seen in future experiments.

The main advantage of this heavy system is the existence of the α -decay phenomenon. The formation amplitude for transitions between ground states $I_\nu = 0_1^+$ is given in Fig. 2. One notices the peak on the nuclear surface denoting that the α -particle is indeed created at small densities. By using the formation amplitude as a wave function satisfying some Schrödinger equation, it is possible to estimate the local equivalent potential corresponding to this solution. It is given in Fig. 3 by a solid line. It has indeed a pocket-like molecular shape used by several phenomenological approaches [8].

3 Matching conditions

The decay width can be estimated by using the well known expression [8]

$$\Gamma = \hbar v \left[\frac{f_{int}(R)}{f_{ext}(R)} \right]^2 = P(R)\gamma^2(R) \sim const , \quad (3.1)$$

in terms of the Coulomb penetrability and reduced width

$$\begin{aligned} P(R) &= \frac{2\rho}{f_{ext}^2(R)} \\ \gamma^2(R) &= \frac{\hbar^2}{2\mu R} f_{int}^2(R) . \end{aligned} \quad (3.2)$$

The general matching condition between the internal and external wave functions for a spherical emitter can be written in terms of the logarithmic derivative

$$\frac{f'_{int}(R)}{f_{int}(R)} = \frac{f'_{ext}(R)}{f_{ext}(R)} . \quad (3.3)$$

In principle Eqs. (3.1) and (3.3) should not depend upon the radius R , i.e. the internal microscopic and external phenomenological solutions should be parallel, at least for some region between the touching configuration and Coulomb barrier. This common condition, called “plateau condition”, is automatically satisfied when both internal and external components are provided as one solution of the Schrödinger equation. In our case the internal solution is provided by the amplitude (2.4) and the proof of the “plateau condition” is a test of validity for the microscopic approach. This task is difficult to achieve for two main reasons.

(i) The microscopic estimate of the formation amplitude in terms of two-proton and two-neutron orbitals provided by the above described microscopic procedure gives a decay width by two orders of magnitude smaller than the experimental value.

(ii) The external logarithmic derivative is proportional to the Coulomb parameter χ . Indeed, the external solution $f_{ext}(R)$ beyond the barrier region is proportional to the irregular Coulomb wave G_0 , because the regular solution practically vanished here and a very good estimate (within a 2% error) is given by the WKB ansatz

$$\begin{aligned} G_l(\rho, \chi) &\approx G_0(\rho, \chi) C_l \\ G_0(\rho, \chi) &= (ctg \alpha)^{1/2} exp[\chi(\alpha - \sin \alpha \cos \alpha)] \\ C_l &= exp\left[\frac{l(l+1)}{\chi} \sqrt{\frac{\chi}{\rho} - 1}\right] , \end{aligned} \quad (3.4)$$

where

$$\cos^2 \alpha \equiv \frac{\rho}{\chi} = \frac{Q}{V_C(R)} = \frac{QR}{2Ze^2} < 1 . \quad (3.5)$$

It turns out that the internal formation amplitude, provided by the above described microscopic procedure, is insensitive to this parameter.

4 Hybrid single particle basis

This drawback can be cured by using a hybrid basis containing an α -cluster component in addition to the standard sp basis $\psi_{\tau eljm}(\mathbf{x}) = \langle \mathbf{x} | c_{\tau eljm}^\dagger \rangle$, $\mathbf{x} \equiv (\mathbf{r}, s)$, provided as an eigenstate of the standard mean field

$$\psi_{sp} = \psi_{\tau eljm} + \psi_{\tau clus} . \quad (4.1)$$

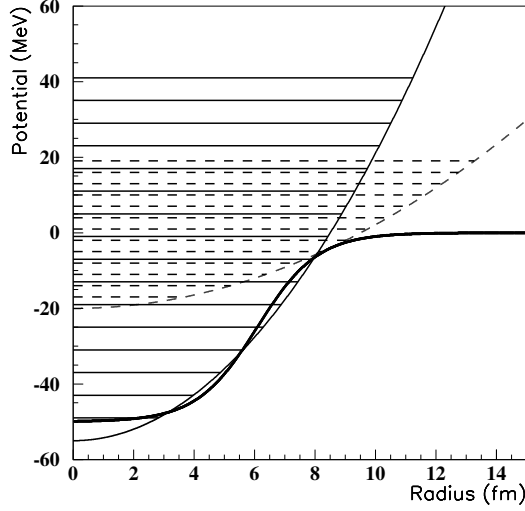


Figure 4: Two ho potential wells generating the hybrid sp basis (4.1). Solid curve generates standard sp orbitals, while the dashed curve is responsible for the cluster component [13].

This idea was employed in Ref. [14], by using a cluster component of about 30% in order to describe the experimental decay width of ^{212}Po . Anyway, the condition (ii) was not fulfilled, because only one emitter was analyzed. Notice in this context that the microscopic formation amplitude (2.15) contains the ho function, depending on four times the ho parameter β . This is due to the fact that sp proton ($\tau = p$) and neutron ($\tau = n$) orbitals are expanded in terms of a ho basis with the parameter β

$$\psi_{\tau eljm}(\mathbf{x}) = \sum_{N=2n+l=0}^{N_0} a_{\tau en} \left[\phi_{nl}^{(\beta)}(\mathbf{r}) \otimes \chi_{\frac{1}{2}}(s) \right]_{jm}, \quad (4.2)$$

depending on the radial quantum number n .

In order to achieve both matching conditions (i) and (ii) we expand the cluster wave function in a similar way

$$\psi_{clus}(\mathbf{x}) = \sum_{N=2n+l=N_0+1}^{N_1} a_{en} \left[\phi_{nl}^{(\beta_c)}(\mathbf{r}) \otimes \chi_{\frac{1}{2}}(s) \right]_{jm}, \quad (4.3)$$

but depending on a different ho parameter β_c [13, 15]. In order to ensure a larger radial tail of the sp orbital, providing a larger value of the decay width, the second

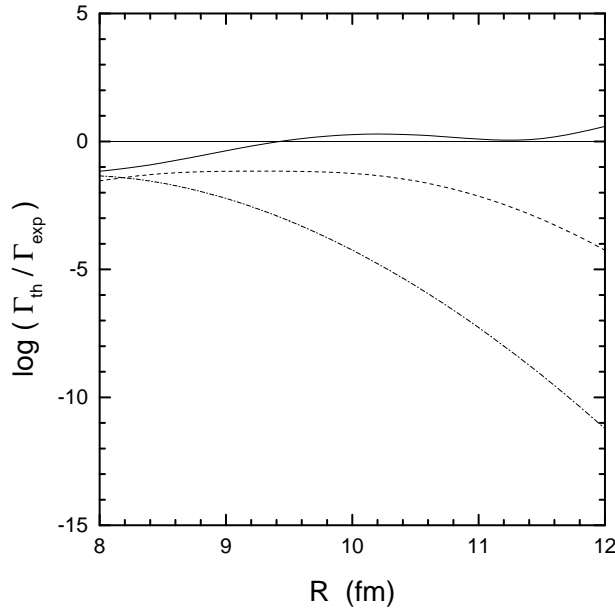


Figure 5: Logarithm of the ratio between the theoretical decay width and the experimental value versus radius if one considers $N_0 = 2n + l = 6$ major shells (dot-dashed curve), $N_1 = 9$ shells with $f = 1$ (dashed curve) and $f = 0.2$ (solid curve) for the last three major shells [15]. The decay process in $^{212}\text{Po} \rightarrow ^{208}\text{Pb} + \alpha$.

ho parameter

$$\beta_c = f\beta, \quad (4.4)$$

should be smaller, i.e. $f < 1$, thus corresponding to a larger ho well, as seen in Fig. 4 (dashed curve). Notice that the solid ho well generates standard sp orbitals.

In Fig. 5 we analyzed the logarithm of the ratio between the theoretical decay width and the experimental value for the decay process in $^{212}\text{Po} \rightarrow ^{208}\text{Pb} + \alpha$ versus radius by considering $N_0 = 2n + 1 = 6$ major shells in the diagonalisation procedure (dot-dashed curve), $N_1 = 9$ major shells with $f = 1$ (dashed curve) and $f = 0.2$ for the last three major shells (solid curve) [15]. In the first two cases the dependence versus radius is strong and the decay width underestimated, while in the last case the dependence becomes quasiconstant and the experimental width is reproduced in the barrier region $R \in [10, 12]$ fm.

In Ref. [7] we performed a systematic analysis of α -decay widths between ground states of even-even nuclei. We used the pairing approach in order to determine two-body X-coefficients. Details are given in Section 5.1. It turns out that more than 90% of the decay width is given by the cluster part of the expansion (4.1) with $f \sim 0.7$. On the other hand, the condition (ii) is fulfilled if one considers the

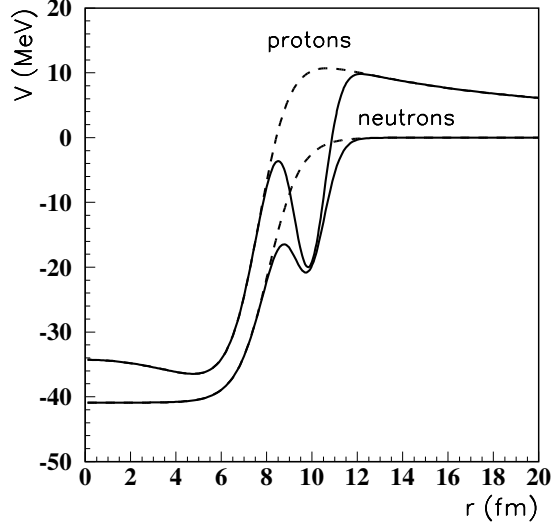


Figure 6: Proton and neutron potentials in ^{216}Rn (solid lines) and the corresponding Woods-Saxon mean-field potentials (dashed lines) [16]. The cluster parts are as in Eq. (4.5) with parameters $b_c = 1$ fm, and $r_c = 1.3(A^{1/3} + 4^{1/3})$ fm.

relation $\beta_c \sim \chi$, due to the fact that the logarithmic derivative of the internal wave function (peaked on the nuclear surface) is proportional to the cluster ho parameter β_c , while the external wave function is proportional to the Coulomb parameter χ .

Let us stress on the fact that we kept unchanged the parameters of the Woods-Saxon potential and changed only the ho parameter for the last shells, describing sp orbitals at large distances. This hybrid basis can be generated in a natural way by considering the standard Woods-Saxon mean field plus a Gaussian correction on the nuclear surface [16]

$$\begin{aligned}
 V^\tau(r) &= V_{WS}^\tau(r) + V_{clus}^\tau(r) \\
 V_{clus}^\tau(r) &= V_\alpha^\tau \exp \left[- \left(\frac{r - r_c}{b_c} \right)^2 \right] \\
 V_{clus}^p - V_{clus}^n &= V_{Coul}(r_c) .
 \end{aligned} \tag{4.5}$$

The potentials for proton and neutrons are plotted in Fig. 6 by solid curves. In Ref. [16] it was shown that the Woods-Saxon part of this potential provides the low-energy and relatively low-spin states that describe spectroscopic properties, while the pocket-like part provides high-energy states with high spin, describing the decay process. In Fig. 7 (a) we plotted the proton cluster strength $-V_{clus}^p$ satisfying the

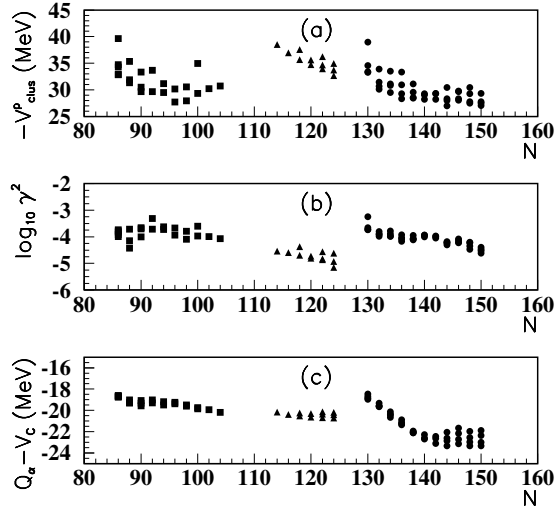


Figure 7: (a) Proton clustering strength $-V_{clus}^p$ as a function of the neutron number for $Z < 82$, $82 < N < 126$ (squares), $Z > 82$, $82 < N < 126$ (triangles), and $Z > 82$, $N > 126$ (circles) [16]. (b) Logarithm of the reduced width at the touching configuration vs neutron number N . (c) The difference between the Q-value and Coulomb barrier vs N .

“plateau condition”

$$\frac{1}{2\Delta R} \int_{R_B - \Delta R}^{R_B + \Delta R} \log_{10} \frac{\Gamma(R)}{\Gamma_{exp}} dR = 0, \quad (4.6)$$

in the barrier region, versus neutron number for various regions between magic numbers. It can be seen that the dependence of the cluster strength is similar to the reduced width plotted in the panel (b) and minus the fragmentation potential $-V_{frag} \equiv -(V_B - Q)$, plotted in the panel (c).

5 Proton-neutron versus α -like correlations

In Ref. [12] we analyzed the influence of proton-neutron correlations on α -decay in the region above ^{100}Sn . The spectroscopic factors in this region have indeed the largest values. One possible reason is the enhancement of the proton-neutron residual interaction, due to the fact that proton and neutron valence orbitals correspond to the same major shell.

5.1 Formation amplitude

The amplitude for the decay process of the parent nucleus into one α -cluster and a daughter nucleus is given by the overlap integral (2.1). The internal α -particle wave function is given by the relative-motion factor of the product between two-proton and two-neutron lowest harmonic oscillator states with the parameter $\beta_\alpha \approx 0.5 \text{ fm}^{-2}$ [4]. For sufficiently large inter-fragment distances with a weak overlap of nuclear densities, the factorization (2.3) is valid for the parent wave function and the formation amplitude simplifies to (2.4). We look for the form of the α -like quartet Ψ_α in the Fock space representation as

$$\begin{aligned} \mathcal{P}_\alpha^\dagger &= \sum_{L_1, L_2} Z_{ppnn}(L_1, L_2) \left[\mathcal{P}_{ppL_1}^\dagger \otimes \mathcal{P}_{nnL_2}^\dagger \right]_0 \\ &+ \sum_{L_1, L_2} Z_{pnpn}(L_1, L_2) \left[\mathcal{P}_{pnL_1}^\dagger \otimes \mathcal{P}_{pnL_2}^\dagger \right]_0, \end{aligned} \quad (5.1)$$

expressed in terms of the coherent pairs

$$\mathcal{P}_{\tau_1 \tau_2 LM}^\dagger = \sum_{j_1 j_2} X_{\tau_1 \tau_2}(j_1 j_2; L) P_{LM}^\dagger(\tau_1 j_1 \tau_2 j_2), \quad (5.2)$$

where

$$P_{LM}^\dagger(\tau_1 j_1 \tau_2 j_2) = \frac{1}{\sqrt{1 + \delta_{\tau_1 \tau_2} \delta_{j_1 j_2}}} \left[c_{\tau_1 j_1}^\dagger \otimes c_{\tau_2 j_2}^\dagger \right]_{LM}. \quad (5.3)$$

We shall use the fact that the second term of Eq. (5.1), representing the contribution of proton-neutron pairs, may be recoupled to a standard proton-proton and neutron-neutron form, i.e.

$$\left[c_{pj}^\dagger \otimes c_{nj}^\dagger \right]_0 \left[c_{pj'}^\dagger \otimes c_{nj'}^\dagger \right]_0 = -\frac{1}{\hat{j} \hat{j}'} \sum_l \hat{l} \left[\left[c_{nj}^\dagger \otimes c_{nj'}^\dagger \right]_l \otimes \left[c_{pj}^\dagger \otimes c_{pj'}^\dagger \right]_l \right]_0. \quad (5.4)$$

By using the spherical symmetry, the form of the quartet becomes

$$\begin{aligned} \mathcal{P}_\alpha^\dagger &= Z_{ppnn} \sum_j X_{pp}(jj; 0) \frac{1}{\sqrt{2}} \left[c_{pj}^\dagger \otimes c_{pj}^\dagger \right]_0 \sum_{j'} X_{nn}(j'j'; 0) \frac{1}{\sqrt{2}} \left[c_{nj'}^\dagger \otimes c_{nj'}^\dagger \right]_0 \\ &- Z_{pnpn} \sum_{j, j', l, m} \frac{\hat{l}}{\hat{j} \hat{j}'} X_{pn}(jj; 0) X_{pn}(j'j'; 0) \left[\left[c_{nj}^\dagger \otimes c_{nj'}^\dagger \right]_l \left[c_{pj}^\dagger \otimes c_{pj'}^\dagger \right]_l \right]_0. \end{aligned} \quad (5.5)$$

We perform the overlap integral by using the coordinate representation

$$\begin{aligned} \left[c_{j_1}^\dagger \otimes c_{j_2}^\dagger \right]_{LM} &\rightarrow \mathcal{A} \{ \psi_{j_1}(\mathbf{x}_1) \otimes \psi_{j_2}(\mathbf{x}_2) \} \\ &= \frac{1}{\sqrt{2}} \{ [\psi_{j_1}(\mathbf{x}_1) \otimes \psi_{j_2}(\mathbf{x}_2)]_{LM} - [\psi_{j_1}(\mathbf{x}_2) \otimes \psi_{j_2}(\mathbf{x}_1)]_{LM} \}. \end{aligned} \quad (5.6)$$

We then use the ho representation

$$\psi_{\tau\epsilon ljm}(\mathbf{x}) = \sum_n c_n(\tau\epsilon ljm)\phi_{nljm}^{(\beta)}(\mathbf{x}), \quad (5.7)$$

where we considered the sp basis within the jj scheme

$$\begin{aligned} \phi_{nljm}^{(\beta)}(\mathbf{x}) &= \left[\phi_{nl}^{(\beta)}(\mathbf{r}) \otimes \chi_{\frac{1}{2}}(s) \right]_{jm} \\ \phi_{nl}^{(\beta)}(\mathbf{r}) &= \mathcal{R}_{nl}^{(\beta)}(r) i^l Y_{lm}(\hat{r}). \end{aligned} \quad (5.8)$$

By using the recoupling to the LS scheme, the changing from absolute to relative and cm proton and neutron pair coordinates, and then by recoupling to relative and cm α -coordinates one obtains the following result

$$\mathcal{F}(\mathbf{R}) = \sum_{N_\alpha} W(N_\alpha) \phi_{N_\alpha 0}^{(4\beta)}(\mathbf{R}), \quad (5.9)$$

where

$$\begin{aligned} W(N_\alpha) &= Z_{ppnn} \sum_{N_p, N_n} G_p(N_p) G_n(N_n) \langle n_\alpha 0 N_\alpha 0; 0 | N_p 0 N_n 0; 0 \rangle \mathcal{I}_{n_\alpha 0}^{(\beta, \beta_\alpha)} \\ &- Z_{pnpn} \sum_{N_p, N_n, L} G_{pn}(N_p, N_n, L) \langle n_\alpha 0 N_\alpha 0; 0 | N_p L N_n L; 0 \rangle \mathcal{I}_{n_\alpha 0}^{(\beta, \beta_\alpha)}. \end{aligned} \quad (5.10)$$

The G coefficients contain all recoupling transformations. The $ppnn$ coefficients are

$$\begin{aligned} G_\tau(N_\tau) &= \sum_{n_1 n_2 j} B_\tau(n_1 n_2 j) \langle (ll) 0 (\frac{1}{2} \frac{1}{2}) 0; 0 | (l \frac{1}{2}) j (l \frac{1}{2}) j; 0 \rangle \\ &\times \sum_{n_\tau} (-)^l \langle n_\tau 0 N_\tau 0; 0 | n_1 l n_2 l; 0 \rangle \mathcal{I}_{n_\tau 0}^{(\beta, \beta_\alpha)}, \quad \tau = p, n, \end{aligned} \quad (5.11)$$

while for the $pnpn$ part we have

$$\begin{aligned} G_{pn}(N_p, N_n, L) &= \sum_{j, j'} \hat{L} X_{pn}(jj; 0) X_{pn}(j'j'; 0) B_{pn}(jj'; N_p, L) B_{pn}(j'j'; N_n, L) \\ &\times \langle (jj') L (\frac{1}{2} \frac{1}{2}) 0; L | (l_j \frac{1}{2}) j (l_{j'} \frac{1}{2}) j'; L \rangle^2. \end{aligned} \quad (5.12)$$

They are expressed in terms of the coefficients

$$\begin{aligned} B_\tau(n_1 n_2; j) &= X_{\tau\tau}(jj; 0) c_{n_1}(\tau j) c_{n_2}(\tau j), \\ B_{pn}(jj'; N_\tau, L) &= \sqrt{2} \sum_{n_\tau, n_1 n_2} c_{n_1}(\tau j) c_{n_2}(\tau j') i^{l_j + l_{j'}} \langle n_\tau 0 N_\tau L; L | n_1 l_j n_2 l_{j'}; L \rangle \mathcal{I}_{n_\tau 0}^{(\beta, \beta_\alpha)}. \end{aligned} \quad (5.13)$$

5.2 Pairing correlations

We will consider in our analysis a schematic isovector pairing Hamiltonian with constant strengths

$$H = \sum_{\tau=p,n} \sum_j \epsilon_{\tau j} N_{\tau j} - \sum_{\mu=pp,nn,pn} \frac{G_\mu}{2} \sum_{jj'} \hat{j} \hat{j}' P_{\mu j}^\dagger P_{\mu j'} , \quad (5.14)$$

given in terms of the number of particles and the pair operators of Eq. (5.3)

$$\begin{aligned} N_{\tau j} &= \sum_{m>0} (c_{\tau j m}^\dagger c_{\tau j m} + c_{\tau j \overline{m}}^\dagger c_{\tau j \overline{m}}) , \\ P_{pp}^\dagger &= P_{00}^\dagger (p j p j) , P_{nn}^\dagger = P_{00}^\dagger (n j n j) , P_{pn}^\dagger = P_{00}^\dagger (p j n j) . \end{aligned} \quad (5.15)$$

5.3 pn-BCS treatment

When taking into account proton-neutron correlations, the quasiparticles carry an additional degree of freedom as the full Bogoliubov transformation also mixes protons and neutrons

$$b_{kjm}^\dagger = \sum_{\tau=pn} (u_{k\tau j} c_{\tau j m}^\dagger - v_{k\tau j} c_{\tau j \overline{m}}) , \quad k = 1, 2 . \quad (5.16)$$

As a particular case, one recovers the decoupled BCS version for protons $k = 1$, $\tau = p$ and neutrons $k = 2$, $\tau = n$, respectively. The pairing gaps read

$$\begin{aligned} \Delta_\tau &= G_{\tau\tau} \sum_{kj} \frac{2j+1}{2} u_{k\tau j} v_{k\tau j} , \quad \tau = p, n , \\ \Delta_{pn} &= G_{pn} \sum_{kj} \frac{2j+1}{2} \frac{u_{knj} v_{kpj} + u_{kpj} v_{knj}}{2} . \end{aligned} \quad (5.17)$$

The coherent BCS pair amplitudes of Eq. (5.2) are given by

$$\begin{aligned} X_{\tau,j} &= \frac{1}{2} \langle D | [c_{\tau,j} c_{\tau,j}]_0 | P \rangle = \frac{\sqrt{2j+1}}{2} \sum_k u_{k\tau j} v_{k\tau j} , \quad \tau = p, n , \\ X_{pn,j} &= \frac{1}{2} \langle D | [c_{pj} c_{nj}]_0 | P \rangle = \frac{\sqrt{2j+1}}{2} \sum_k \frac{u_{knj} v_{kpj} + u_{kpj} v_{knj}}{2} . \end{aligned} \quad (5.18)$$

For the α -like quartet to be isoscalar we require

$$Z_{ppnn} = \frac{2}{\sqrt{3}} , \quad Z_{pnpn} = -\frac{1}{\sqrt{3}} . \quad (5.19)$$

5.4 Exact solutions

In the case of single species pairing ($G_{pn} = 0$), we may easily find the form of the ground state by diagonalising the Hamiltonian in the $2n$ -particle basis. A generic state is written as

$$|\psi_n\rangle = \sum_{i_1 \geq \dots \geq i_n} x_{i_1 \dots i_n}^{(n)} P_{i_1}^\dagger \dots P_{i_n}^\dagger |0\rangle, \quad (5.20)$$

where $P_i^\dagger = \frac{1}{\sqrt{2}} [c_j^\dagger \otimes c_j^\dagger]_0$.

As far as the static properties are concerned, the BCS and diagonalisation treatments are shown below to agree well. However, the coherent pair amplitudes $X_{\tau j}$ are generally overestimated by the BCS treatment.

In Fig. 8 we plotted the exact diagonalization results for $Z = N = 52$ by using a decoupled basis for proton and neutrons (dashes) and coupled pn basis (solid line). These results are indeed larger in comparison with the BCS (dashes) and pn-BCS cases (thick solid line), but still they underestimate the experimental decay widths.

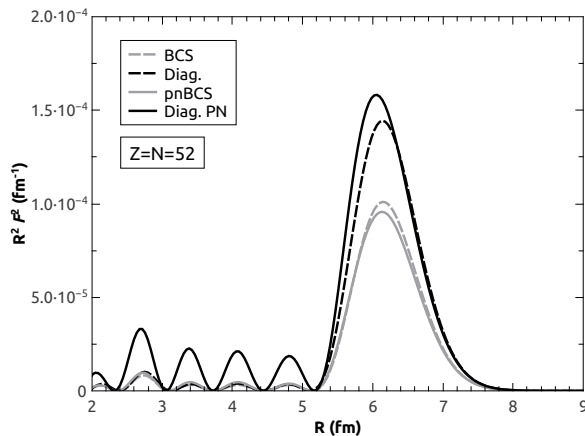


Figure 8: Comparison of formation amplitudes in various approaches. The proton spectrum is considered identical to the neutron spectrum [12].

As we already pointed out, the standard mean-field approach cannot supply enough four-body correlations to form an α -particle on the nuclear surface, because the computed decay widths are too small. One convenient way to simulate the missing four-body correlations was described in the previous Section by considering an additional Gaussian pocket-like attractive component on the surface region of the single-particle mean field [16]. We considered such a component in both proton and neutron mean fields with the same parameters

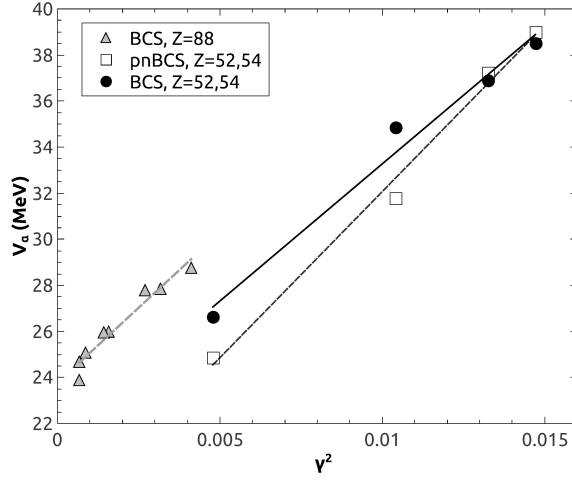


Figure 9: The strength of the α -clustering additional part of the mean field potential V_α versus the reduced width [12].

By adjusting the strength of this component V_α , it is possible to reproduce the experimental decay widths. In Fig. 9, we plotted this strength within the BCS approach versus the experimental reduced width for the region above ^{100}Sn (triangles) and above ^{208}Pb (solid circles). One remarks that these values are proportional, due to the fact that they were simultaneously determined. Thus, the strength of the additional potential is greater for lighter nuclei with $Z \sim N$. Let us mention that we obtained similar values for light nuclei by using the pn-BCS approach (open squares). Therefore the pn correlations are not able to explain larger reduced widths for $N \sim Z$ nuclei above ^{100}Sn . The fitted values plotted by the corresponding lines in Fig. 9 have similar slopes and intercepts. This feature proves the universal character of the α -clustering across the nuclear chart.

6 Conclusions

We explained the α -like rotational bands in the $^{40}\text{Ca}+\alpha$ system by computing the α -formation amplitude in terms of single particle Gamow resonances. We demonstrated that the systematics of decay widths between ground states cannot be explained in terms of a collective four-body state built from two-proton and two-neutron orbitals of the standard nuclear mean field. It can be understood only in terms of a preformed α -cluster existing on the nuclear surface in addition to the above mentioned mean field cluster. Therefore, we used a semi-microscopic hybrid model combining the mean field formation with a preformed α -cluster in order to explain the order of magnitude of the experimental decay width. We compared

proton-neutron with α -like correlations above the double magic nucleus ^{100}Sn . Finally we evidenced the universal character of α -like correlations.

References

- [1] G. Gamow, Z. Phys. **51**, 204 (1928).
- [2] E.U. Condon and R.W. Gurney, Nature **122**, 439 (1928).
- [3] A.M. Lane and R.G. Thomas, Rev. Mod. Phys. **30**, 257 (1958).
- [4] H.J. Mang, Phys. Rev. **119**, 1069 (1960).
- [5] A. Săndulescu, Nucl. Phys. A **37**, 332 (1962).
- [6] D.S. Delion and A. Săndulescu, J. Physics G **28**, 617 (2002).
- [7] D.S. Delion, A. Săndulescu, and W. Greiner, Phys. Review C **69**, 044318 (2004).
- [8] D.S. Delion, *Theory of particle and cluster emission* (Springer-Verlag, Berlin, 2010).
- [9] D. S. Delion, Phys. Rev. C **80**, 024310 (2009).
- [10] D.S. Delion and J. Suhonen, Phys. Rev. C **61**, 024304 (2000).
- [11] D.S. Delion and J. Suhonen, Phys. Rev. C **63**, 061306 (2001).
- [12] V.V. Baran and D.S. Delion, Phys. Rev. C **94**, 034319 (2016).
- [13] D.S. Delion, A. Insolia, and R.J. Liotta, Phys. Rev. C **54**, 292 (1996).
- [14] K. Varga, R. G. Lovas, and R. J. Liotta, Nucl. Phys. A **550**, 421 (1992).
- [15] D.S. Delion, Rom. J. Phys. **39**, 645 (1994); **40**, 25 (1995).
- [16] D.S. Delion and R.J. Liotta, Phys. Rev. C **87**, 041302 (2013).